Available online at www.sciencedirect.com
SCIENCE DIRECT®
Biomaterials 25 (2004) 1177–1186
Biomaterials
www.elsevier.com/locate/biomaterials

Significance of melt-fraction in HVOF sprayed hydroxyapatite particles, splats and coatings

K.A. Khor[a,*], H. Li[a], P. Cheang[b]

[a] School of Mechanical and Production Engineering, Advanced Materials Research Centre, Nanyang Technological University, 50 Nanyang Avenue, Singapore 639798, Singapore

[b] School of Materials Engineering, Advanced Materials Research Centre, Nanyang Technological University, 50 Nanyang Avenue, Singapore 639798, Singapore

Received 10 January 2003; accepted 11 August 2003

Abstract

Microstructure characterization and property evaluation of high velocity oxy-fuel (HVOF) sprayed hydroxyapatite (HA) splats and coatings were conducted in the present study as a function of the proportion of melting that occurred in HA particles during HVOF spray. In vitro behavior of single and folded HA splats in simulated body fluid was also investigated. Results showed that phase composition of as-sprayed HA coatings was influenced significantly by the melt fraction in HVOF sprayed particles. Melt fraction of the HA powders were experimentally determined from particle morphology analysis. It was found that the spray parameters and starting powder size influenced the melt fraction of the particles. In vitro investigation of individual HA splats made from different HA particles revealed decisive role of local phase composition in influencing their dissolution/precipitation behavior during the test. Furthermore, Raman spectroscopy qualitative inspection on the sprayed HA particles (partial melted) revealed that thermal decomposition occurred within the melted part rather than the unmelted zone. Young's modulus and micro-hardness of the as-sprayed particles and coatings were determined using nano-indentation technique. The resolidified zone of the sprayed HA particles exhibited an average Young's modulus value of 41.25 GPa. The measured values ranged from 23.1 to 65.3 GPa. The unmelted part of the HA powders showed a markedly narrower range. Young's modulus value of 83.9 GPa ($\pm$9.4 GPa) was recorded for this region. This succinctly highlight the difference between the unmelted region and melted regions of a HA particle. Young's moduli values measured on HVOF coatings were found to mirror the trend found in the spheroidised particles and splats with apt fidelity.

Keywords: Hydroxyapatite; HVOF; Splat; In vitro; Melt state

1. Introduction

Hydroxyapatite (HA) coatings deposited using thermal spray techniques on titanium alloy substrates showed capability of avoiding the inherent mechanical property limitations of bulk HA without remarkable loss in biocompatibility [1,2]. In order to elucidate the potential of HA in clinical applications, extensive investigations on thermal sprayed HA coatings have been conducted mostly through in vitro and in vivo tests [3–7]. The bioactivity of thermal sprayed HA coatings has been generally disclosed through previous studies [3,4,8–10]. It was found that the macro- and micro-structure of HA was particularly important for the apposition of bone [11]. The biological performance of the calcium phosphate coatings was essentially phase-dependent and, biological behavior of the phases in the calcium phosphate family has been largely elucidated [12,13]. It is therefore postulated that optimization of the phase composition of as-sprayed calcium phosphate coatings is a prerequisite towards their competitive applications. Owing to its relatively low flame temperature ($<2800^{\circ}C$) and high flame velocity, high velocity oxy-fuel (HVOF) technique showed potential for depositing highly dense HA coatings. The advantages of HA coatings deposited using HVOF lie in diminished phase transformation of HA, and enhanced mechanical properties compared to those deposited using plasma spray. It should be noted that the extent of thermal

*Corresponding author. Tel.: +65-790-5526; fax: +65-791-1859.
E-mail address: mkakhor@ntu.edu.sg (K.A. Khor).

0142-9612/$ - see front matter © 2003 Elsevier Ltd. All rights reserved.
doi:10.1016/j.biomaterials.2003.08.008

decomposition of HA to tricalcium phosphate (TCP), tetracalcium phosphate (TTCP), or amorphous calcium phosphate (ACP) is closely related to the heat input, and hence the melt state of HA particles during coating deposition [14–16]. The term 'melt-state' refers arbitrarily to the extent of melting that took place in the particles prior to impact, and subsequent solidification on the substrate. It would be possible that the phase composition, and, properties of resultant HA coatings can be achieved through the control of the melt state of HA particle in the HVOF flame. Since it is difficult to accurately determine the melt state of HA from microstructure analysis of bulk coating, examination made on individual sprayed HA particles and splats is performed in this study.

Thermal sprayed coating is composed of liquid droplets that rapidly solidified upon impact. Occasionally, the droplets might partially solidify prematurely prior to impact. It is likely that some droplets will contain entrapped gases. Furthermore, it is well known that thermal sprayed coating shows a layered structure, which is a splat-accumulated structure. Apart from the influence of residual stresses, which is generated during coating formation, properties of the bulk coating are essentially derived from the characteristics of the solidified splats, which are fundamentally the basic units in the thermal sprayed coatings [17–19]. Therefore, the study on the properties of sprayed particles and splats are essentially important. Extensive studies have been focused on morphology characterization of the thermal sprayed splats [20–22]. However, property evaluation is still acutely lacking, mainly due to the limitation of existing testing techniques. Moreover, the overall in vitro behavior of bulk HA coating should be directly related to that of separate HA splats. A good understanding of the in vitro behavior of single HA splat would significantly contribute to the knowledge on dissolution/precipitation mechanism of HA coatings. In the present study, HVOF sprayed HA powders were collected for structure characterization and property evaluation. Furthermore, isolated HA splats were also deposited on polished Ti–6Al–4V substrates and subsequently immersed into simulated body fluid (SBF) for investigation.

2. Experimental procedures

Spray dried HA (SDHA) powders made from a wet chemical method [23] were employed for the spraying. The powders were only composed of crystalline HA, which was ascertained through an annealing treatment at 900°C after the spray drying process. The HA powders were sprayed using a fully computerized HV2000 HVOF system (Praxair Thermal Inc., USA) with a nozzle diameter of 19 mm. Hydrogen (99.9995% in purity) was utilized as the fuel gas combusted in purified oxygen gas (99.8% in purity) and the powder carrier gas was argon (99.998% in purity). Powder feed rate was 6 g/min. In order to achieve the different melt states in the powders, HA powders in different particle size range were prepared through fine sieving. The size range distribution of the powders was analyzed using a laser particle size analyzer (Analysette 22, Fritsch Gmbh, Germany). Before the systematic study of the HVOF HA coatings, extensive preliminary work was conducted in optimizing spray parameters and starting HA powders. It was found that for HVOF spraying, due to its relatively low flame temperature and short in-flight dwelling of the powders during spraying, once the powder size was larger than 75 μm, the heating of the HA powders would be insufficient (very limited melting at the shell of the particles), which resulted in extremely poor bonding of the deposited powders to form a coating. Most of the particles that impacted on the substrate rebounded off. Furthermore, it was revealed that, when the powder size was less than 20 μm, the powders were overheated such that amorphization/decomposition was intensified and the crystallinity was generally $<30\%$. The salient characteristics of the powders and HVOF spray parameters are tabulated in Table 1.

Structure characterization of the powders and coatings was conducted using scanning electron microscopy (SEM, JEOL JSM-5600LV) and transmission electron microscopy (TEM, JEOL, JEM-2010) at 200 kV. Cross sections of the collected powders were ground and polished for the observation under SEM. Phase composition of as-sprayed coatings was qualitatively determined through X-ray diffraction (XRD) analysis (MPD 1880, Philips, the Netherlands). The operating conditions were 40 kV and 30 mA with Cu Kα radiation. The goniometer was set at a scan rate of 0.015° 2θ/s over a 2θ range of 20–60°. A Raman spectroscopy analysis was conducted on polished (1 μm diamond paste) cross-sections of sprayed particles at different locations using a Renishaw Raman imaging microscope WiRE

Table 1
HVOF Spray parameters and coating classification

Coating designation	Flow of oxygen (l/min)	Flow of hydrogen (l/min)	Spray distance (mm)	Powder
C-1	236	519	210	A
C-2	236	519	250	A
C-3	283	519	250	A
C-4	283	566	250	A
C-5	330	566	250	A
C-6	283	566	250	B
C-7	283	566	250	C

Note: Powder A: 50 ± 10 μm, powder B: 40 ± 10 μm, powder C: 30 ± 10 μm.

spectroscopy equipped with 50 mW Class 3B helium–neon laser ($\lambda = 632.816$ nm). The probing spot was about 4 μm in diameter under $\times 1000$ microscope (Lei DML). Quantitative phase analysis on investigated crystalline coatings was conducted using Rietquan program based on the Rietveld method [24]. It has been proved that these methods using structure parameters was significantly more reliable than those using peak separation or total integrated intensities of groups of overlapping peaks [25]. The detailed information for the refinement, e.g., crystal structure information for phases refined by the Rietveld method, refinement principles, etc., has been provided elsewhere [26].

The melt fractions of HVOF sprayed HA powders were experimentally determined through image analysis. It was found that during the present HVOF spraying, most HA powders were only partially melted, which is schematically shown in Fig. 1. After appropriate grinding and polishing, from the figure, the 'melt fraction in particle' (MFP) of HA powders is defined as the ratio of melted volume to the whole particle's volume:

$$\mathrm{MFP} = \frac{V_{\mathrm{melted}}}{V_{\mathrm{total}}} = \frac{R^3 - r^3}{R^3} \times 100\%, \quad (1)$$

where R and r are the radius of HA particle and the unmelted core, respectively. Determination of MFP was performed through deriving the area ratio obtained using the ImagePro image analysis software to volume ratio. From the image analysis, the area ratio of molten part (A) and area of unmelted part (B) can be determined

$$a = \frac{A}{B} = \frac{R^2 - r^2}{r^2}. \quad (2)$$

Combined with the above definition, the melt fraction of alternative HA particles can be calculated according to the following formula:

$$\mathrm{MFP} = 1 - \left(\frac{1}{1+a}\right)^{3/2}. \quad (3)$$

The calcium phosphate splats were collected on polished Ti–6Al–4V plate substrates by using the same HVOF spray process as C-4. The powders with alternative sizes were sprayed to prepare splats with different morphology on the polished Ti substrates. A filter-plate was placed between the substrate and HVOF flame to 'filter' off single HA splats from the spray stream, and several holes of 1 mm in diameter were drilled on the plate. In the present study, the splats were incubated in the SBF for up to 3 days to reveal its dissolution/precipitation behavior. The substrate on which HA splats were deposited used for in vitro test was of the dimension of $12 \times 12 \times 2\,\mathrm{mm}^3$ in width, length and width, respectively. The Kokubo SBF (pH = 7.40) [27] was used for the in vitro incubation. The in vitro test was conducted in a continuously stirred bath containing distilled water with a stable temperature of 37°C. Each sample was incubated in 70 ml SBF contained in a polyethylene bottle. Once the sample was taken out from the solution, it was washed in distilled water and subsequently dried at ambient temperature.

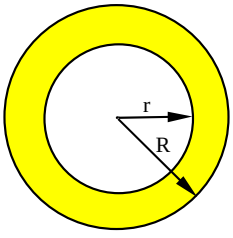

Fig. 1. Sketch of HA particle during HVOF spraying showing partially melted state, R—radius of HA particle, r—radius of unmelted core.

The Young's modulus and microhardness of the sprayed particles were determined through nanoindentation test on Nano-Indenter®XP equipment. The samples were fine polished using 1 μm diamond paste after grinding. Since the nanoindentation test was carried out on small areas of materials, it was believed that local mapping of elastic modulus variations on the size scale of the microstructure was possible [28–30]. The nanoindentation was carried out on the polished cross-sections of the sprayed particles and the coatings. For each sample, a total of 15 data points were collected for an average value. The load used for the present nanoindentation was 30 mN. Furthermore, Young's modulus determination via 3-point bend test, and fracture toughness determination via micro-indentation test, on the coatings was conducted. The test methods have been reported in detail in a previously published report [31]. The adhesive bonding strength testing was carried out according to ASTM C633-79. The testing was conducted using the universal Instron machine with a tensile rate of 1 mm/min.

3. Results and discussion

3.1. Influence of melt fraction on structure of resultant HA coatings

Typical cross-sectional morphology of as sprayed HA particles are shown in Fig. 2. The SEM morphology obviously demonstrates the miscellaneous powders' melt state. It reveals that with the increase of particle size, the melt fraction of the particles decreases. Fig. 3 shows the experimental results on the melt fraction of the powders (MFP) during HVOF spraying. Fine powders (C-7, 30 ± 10 μm) contained MFP values in excess of 90%, while the large powder (C-4; 50 ± 10 μm) have MFP values that stretches down to ~20%. It also shows that apart from the influence of starting powder size, the

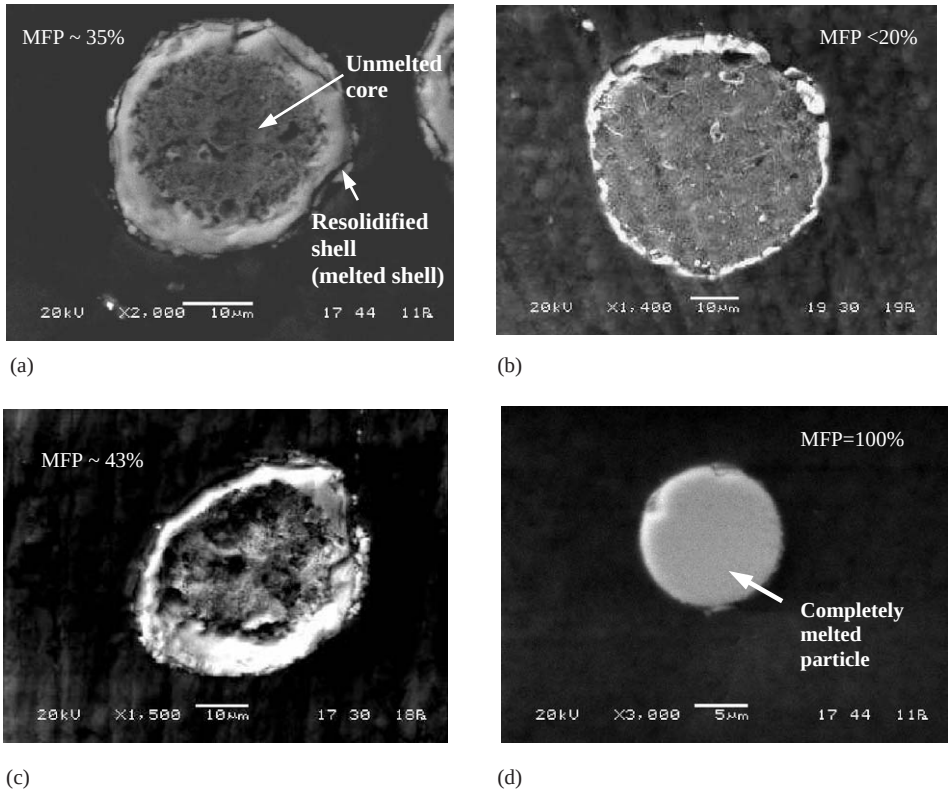

Fig. 2. Cross-sectional morphology of HVOF sprayed HA particles showing their different melting fraction depending on the altered particle size.

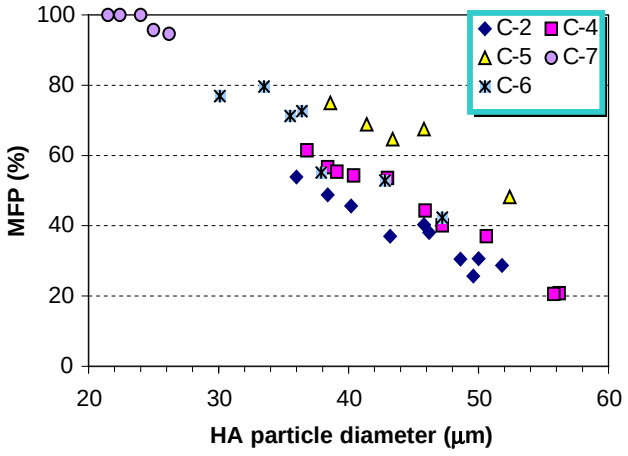

Fig. 3. Melting fraction of HA powders during HVOF spraying, the value was obtained from image analysis on collected HA particles.

increase of flow rate of oxygen and hydrogen, which contributes to an increased flame temperature, also results in increased melt fraction values (cf. C-2 and C-5 in Fig. 3). The result confirms that high oxygen or hydrogen flow rates (330 l/min for oxygen and 566 l/min for hydrogen as in C-5) are beneficial towards achieving adequate melt fraction of HVOF sprayed powders owing to increased heat input, or attaining high flame temperature [32]. Furthermore, the melt-resolidification phenomenon induces a densified structure that compared favorably to the starting powders, which exhibit a porous structure. From this point of view, different melt fractions of HA powders correspond to different coating structures. In order to reveal the influence of different melt state of the powders on phase composition of resultant coatings, the coatings, C-4, C-6 and C-7, were analyzed. Fig. 4 shows the XRD patterns of the three types of coatings. It is found that decrease of powder size results in an increase in ACP phase, and extent of thermal transformation of HA. The following formula was widely suggested to describe the decomposition of HA [15,33,34]

$$Ca_{10}(PO_4)_6(OH)_2 \rightarrow 3Ca_3(PO_4)_2 + CaO + H_2O. \quad (4)$$

The decomposition of HA during coating deposition can result in some CaO simultaneously, but because of the low content (<1 wt%), it could not be detected by XRD analysis. The formation of the ACP was apparently associated with partial dehydroxylation of HA [35] during melting and subsequent rapid solidification of the powders [36]. The melted portion of the powder is in direct response to the formation of ACP. Moreover, crystalline HA phase is generally attributed to the retention of original HA phase in the sprayed powders. For near crystalline coatings (crystallinity >90%, determined arbitrarily from XRD technique [37]), content of α-TCP was determined using the Rietveld method, which is shown in Fig. 5. Content of

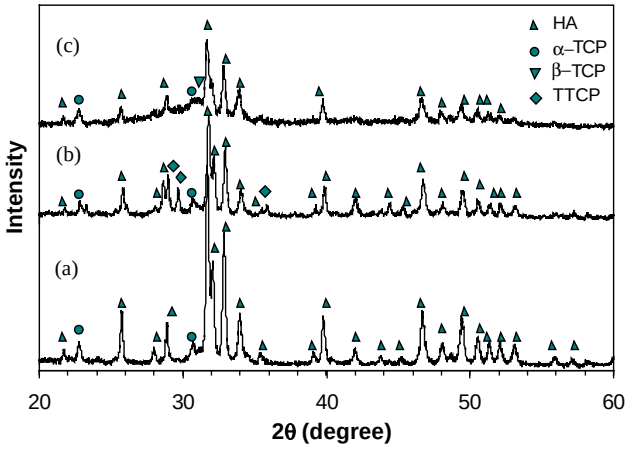

Fig. 4. XRD patterns of the typical calcium phosphate coatings: (a) C-4 coating; (b) C-6 coating; and (c) C-7 coating.

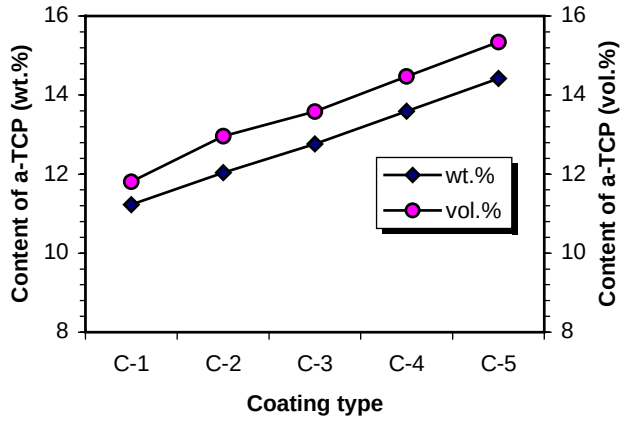

Fig. 5. Content of α-TCP in as-sprayed crystalline coatings showing the influence of spray parameters on phase composition of resultant coatings.

TCP directly reflects the extent of the transformation that occurred following solidification of the droplets on the substrate. It is clear that the high MFP values in C-4 and C-5 corresponds to excessive extent of phase transformation of HA to TCP. Furthermore, for the coatings made from small HA powders, as shown in Fig. 4(b) and (c), TTCP and β-TCP are also present, which suggests that further heating of HA could result in additional phase transformation to TTCP. Liao et al. [38] reported that transformation to TTCP occurred at about 1360°C through some transient phases. It has been found that no transformation to α-TCP from a stoichiometric HA (with a Ca/P ratio of 1.67) could be detected up to 1200°C with prolonged heating [39]. The appearance of β-TCP is possibly attributed to the phase transformation from α-TCP at about 1100°C [40]. It should be noted that TTCP and β-TCP were only detected in the coatings made from small HA powders (such as C-6 and C-7). This may suggest the influence of the melt fraction of HA powder (in the range MFP = 40–100%) on subsequent cooling rate upon impingement, which could determine further phase transformation besides α-TCP. This point was proven by other studies that once HA powders had been totally melted, in the resultant coating, the phases, α-TCP, TTCP and β-TCP, are all exhibited [41]. The difference in the content of α-TCP in the coatings demonstrated in Fig. 5 further indicates that the extent of HA phase decomposition is significantly related to the MFP during coating formation. From this point of view, the melt fraction of powder is practically meaningful. It is clear that augmentation of starting particle size results in decrease in melt fraction hence contributes to decreased phase decomposition of HA. Furthermore, Raman spectra of partially melted HA particles, which are typically shown in Fig. 6, confirm that the phase transformation of HA occurred mainly at the melted part of the particle. The differences between the two curves obtained at melted part and unmelted part, indeed; suggest the significant difference in crystallinity. The broadening and featureless bands between 2000–3600 cm^{-1} are typical features of ACP structure (Raman testing was sensitive with the present amorphous structure). These indicate the predominant presence of uniform ACP phase within the melted part of the sprayed particle. For the unmelted part, the bands of the respective vibration O-P-O modes were narrowed, with an increased intensity and splitting of peaks ($v_2 = \sim 447\,cm^{-1}$, $v_3 = 1040$, $1083\,cm^{-1}$, and $v_4 = 550$, 581, $612\,cm^{-1}$). The main v_1 peak is also observed to have narrowed and shifted from center of $\sim 960\,cm^{-1}$, which is assigned to a typical feature of crystalline HA. The splitting of peaks at v_3 (1047, 1085, and $1118\,cm^{-1}$) suggested the co-existence of HA, α- and β-TCP. The detailed analysis of the Raman peaks can be found elsewhere [42,43]. According to previous studies on HA phase transformation [15,44], the present study suggests that the resolidified shell of the HA particles should contain most of the decomposed phases from HA.

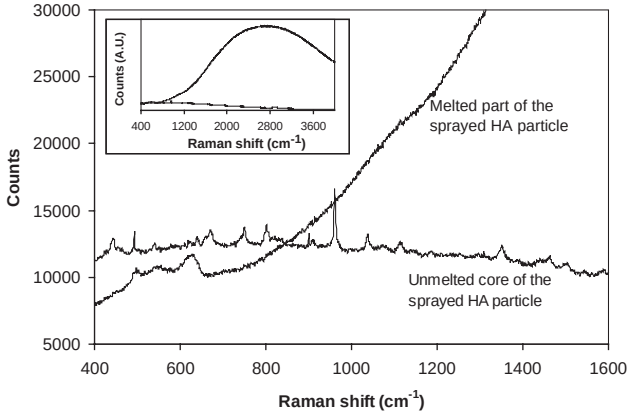

Fig. 6. Typical Raman spectra detected on the polished cross-sections of a partial melted HVOF sprayed HA particle, indicating the main phase transformation of HA at the melted part.

It is evident that partially melted state of HA powders (low MFP values) is beneficial towards obtaining a high crystalline HA coating. Furthermore, phase composition analyses indicate that the melted portion of the particles contained predominantly ACP and TCP. Therefore, in order to effectively inhibit HA decomposition, limited melting of the HA powders must be ensured. It was believed that the high levels in crystallinity of HA coatings were beneficial for long-term survivability, and proper functional life in service with regards to the resolvability of different phases in bony tissues, that is, ACP has a far higher resolvability in the bony tissues than crystalline HA [45]. However, the high resolvability of the amorphous phase is beneficial for accelerated fixation of the implant and, it was also believed that ACP was good for facilitating mechanical mismatch, improving fatigue behavior, and, promoting faster bone remodeling, and hard tissue attachment [46]. In consideration of the above points, HA coatings with a small amorphous content ($<15\%$) would hence be preferred. It should be noted that, during the present HVOF spray study, the particles that have large diameter, i.e. $>30\,\mu m$, are only partially melted. Since the thermal transformation of HA generally occurred at the temperatures beyond 1000°C [44], the melted part of HA particle should contribute strongly to the transformation. The present study indicates that during the HVOF spray, the heating of HA powders is rather limited, which further suggests the suitability of HVOF technique for HA coating deposition.

TEM observation on the coatings reveals the influence of melting-resolidification on grain size, which is shown in Fig. 7. The melted part shows a smaller grain size than the unmelted part. It is noted that the HA grains located in the unmelted part are of far larger size than those in the melted part, which underscores the influence of rapid cooling on grain growth during coating deposition. It should be noted that grain size is mainly responsible for the mechanical performances of materials. The relatively reduced grain size located in the resolidified zone, which is around splats' interface, could act as an important factor contributing to improved mechanical properties.

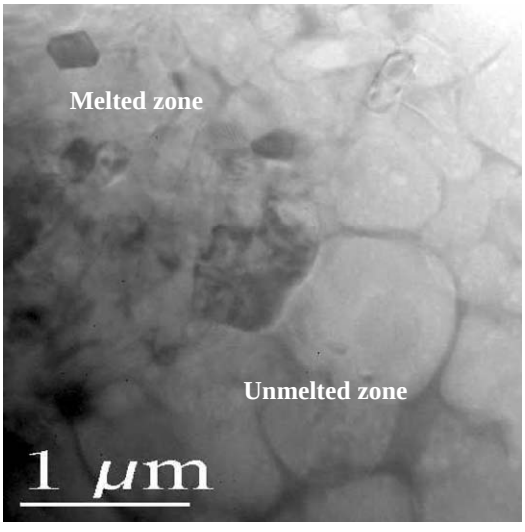

Fig. 7. TEM image of as-sprayed HA coating showing different grain size and the interface between melted and unmelted parts of HA splat.

3.2. In vitro behavior of HA splats

Fig. 8 shows the microstructure changes of HA splats following incubation in vitro. Well-flattened splat morphology suggests fully melted state of HA particle during the HVOF spray. It is found that the original particle size determines its dissolution rate realized through the influence of its melt state. For small HA particles, $\sim 25\,\mu m$, as shown in Fig. 8(a), the resulted splat virtually disappeared, thus indicating complete dissolution before any precipitation commences (Fig. 8(b)). With the augmentation of particle diameter (Fig. 8(c) and (d)), the images clearly demonstrate that the surrounding parts of the splats disappear while the core remained. According to the image analysis, dissolution extent of the splats was determined. The area percentage of dissolved part range from 95% to 5% corresponding to the content of melt fraction in the splats. It has been discussed that TCP and ACP in the as sprayed HA coatings came mainly from melted particles. Even in splats that was heat treated at 450°C for 30 min, it can be seen that the fully melted portion still dissolve away in the SBF despite the annealing treatment, while the unmelted portion remained (Fig. 8(e) and (f)).

During in vitro ageing, TCP and ACP dissolve preferentially into the SBF. It is confirmed that the unmelted portion contains mostly crystalline structure that remained from the starting particle during coating formation. Considering the phase-dependent dissolution of the calcium phosphate phases in SBF [45], the outer layer of single HA splat should contain more dissolvable phases, such as α-TCP, ACP, etc., than sub-terrain layer. The phases coming from HA phase transformation exist mostly around the core based on the consideration that at elevated temperatures, phase transformation occurs [14,39]. With the decrease of HA particle size, under the same spray conditions, high MFP can be achieved, which is responsible for an increased extent of HA phase transformation. The resultant phases should be responsible for the dissolution during immersion in SBF. From this viewpoint, fully melted state of HA particles is not altogether suitable and, partially melted state is preferred. The present results also claim that the dissolution/precipitation behavior of the HA coatings is significantly dependent on their relative rate. Among the calcium

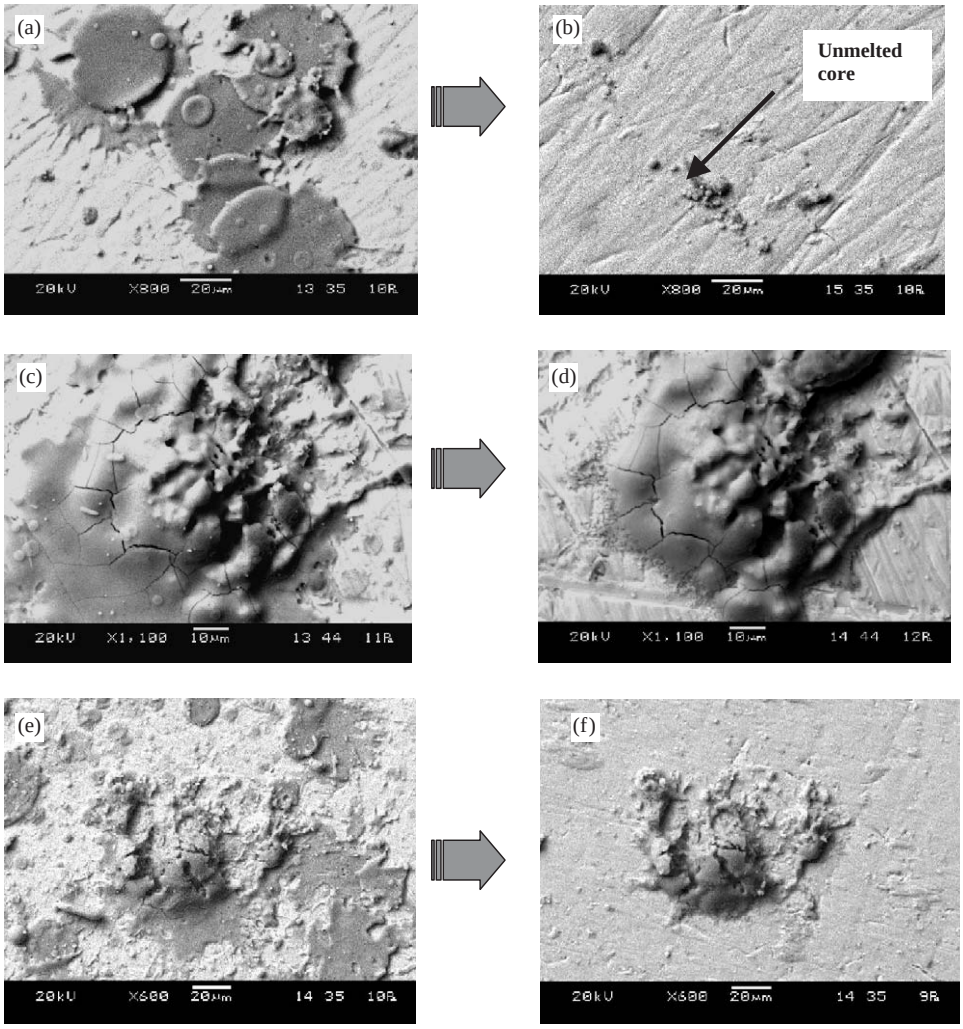

Fig. 8. Images of HA splats before and after immersed in the SBF showing the effect of particle size on the dissolution/precipitation behavior.

phosphate phases, crystalline HA has the highest ratio of precipitation to dissolution. Therefore, for the coatings with some content of crystalline HA, ACP, TCP or TTCP, it is critical to ascertain a proper phase distribution towards achieving a quick precipitation. For a thermal sprayed coating, owing to the randomly distributed splats, an inhomogeneous structure is resulted, which can more or less assure randomly distributed phases. In order to understand the behavior of a bulk HA coating in vitro, multi-splats were also prepared and their dissolution/precipitation phenomena were observed. Fig. 9 shows the morphology changes of the folded splats triggered by 3 days' incubation in the SBF. It is obvious that after 3 days' ageing, remarkable precipitation occurred and the prevention of further dissolution has prevailed at the area with multi-splats. The phenomena indicate that the multi-splats, mostly double folded splats, have significant mutual influence on their overall dissolution/precipitation. In other words, the difference in the rate of dissolution to precipitation can inhibit further dissolution, and hence promote the precipitation. It is noted that, as shown in Fig. 9(a), the well-flattened splats correspond to nearly fully melted particles. As discussed earlier, the splats could consist mostly of dissolvable phases. Compared to the in vitro behavior of single splat, which is shown in Fig. 8, multi-splats show an increased precipitation-to-dissolution rate.

3.3. Young's modulus, adhesion strength, and microhardness

The nanoindentation was carried out on the particles since it is of very limited indentation area as the load is extremely small, which is especially required for the indentation on identified parts within a small HA particle. It should be noted that the overall properties exhibited by bulk HA coating could be mainly attributed to those of separate HA splats. In order to reveal the approximate contribution of different phases, sprayed HA powders were collected and subsequently nanoindentation tests were conducted on their polished

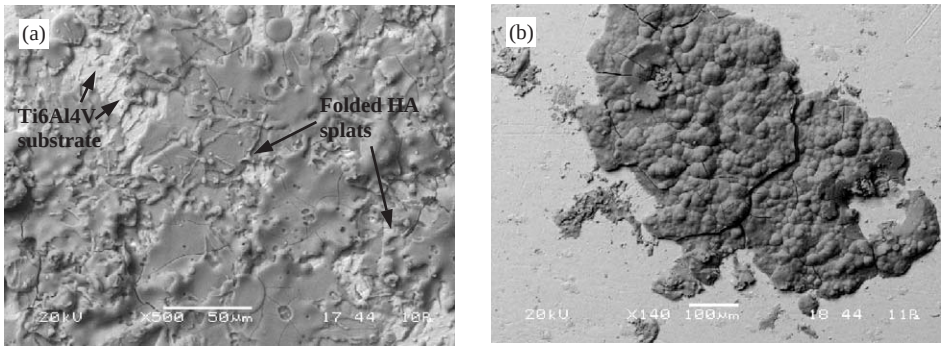

Fig. 9. SEM images of multi-HA splats before (a) and after (b) immersed in the SBF with 3 days showing the mutual effect among the folded splats on the their dissolution/precipitation behavior.

cross-sections. For comparison, the nanoindentation test was also conducted on the polished cross-sections of starting HA powders. Concerning the small indentation area, less than $9 \times 10^4\,nm^2$, the Young's modulus and microhardness data are reliable in reflecting the relations between microstructure and properties.

It was found that different part of the sprayed HA particle exhibits remarkably different Young's modulus. The resolidified zone exhibits an average Young's modulus value of 41.25 GPa with a vast range from 23.1 to 65.3 GPa, which indicates complex phase components within that zone. And the corresponding microhardness shows an average value of 3.37 GPa with a data range from 1.72 to 5.93 GPa. Since the indentation area is extremely small, it is possible that those values reflect the properties of different phases. In other words, the alternation of Young's modulus is attributed to different phases. The unmelted part of the HA powders shows a Young's modulus value of 83.9 ($\pm$9.4 GPa) and a microhardness value of 5.22 ($\pm$0.87 GPa). Since the starting powders were composed of crystalline HA, it can be claimed from the indentation results that crystalline HA exhibits the highest *E*-values. The existence of other phases, such as α-TCP, ACP, could be responsible for the decrease of Young's modulus. The results correspond well to those obtained from bend tests on HA coatings, which was reported in another paper [31]. The present nanoindentation tests further confirmed the significant influence of different phases on overall properties of resultant coatings. It therefore states that optimization of phase components in HA coating is a useful way towards satisfactory mechanical properties. Meanwhile, it is noted that compared to the nanoindentation result on bulk HA coating, which exhibited a Young's modulus of 118 ($\pm$5.21 GPa), the sprayed HA particles showed low Young's modulus. The residual stress formed during coating formation could be responsible for the increased *E*-values exhibited by HA coatings.

Fig. 10 shows that the coatings with relatively high MFP values (C-4, C-5, C-6), and even C-7 where most

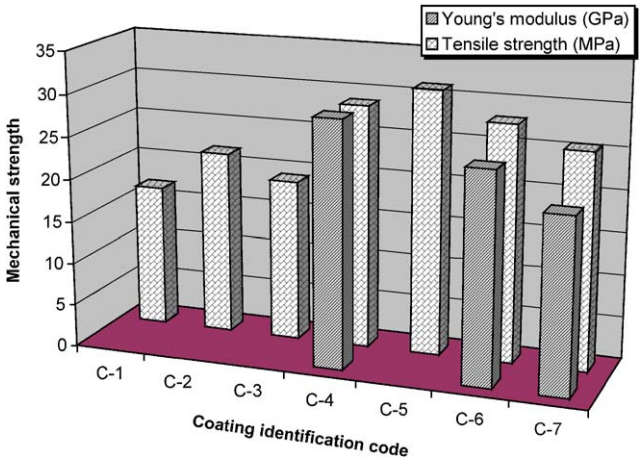

Fig. 10. Adhesive strength and Young's modulus of the as sprayed HA coatings showing the significant influence of spray parameters and starting HA powder size.

of the particles are found to be fully melted (MFP > 90%) have better adhesive bond strength than the coating where the particles have low MFP values (C-2). Indeed, by comparing C-2 and C-5 it can be seen that for practically similar particle size range of 35–55 μm (Fig. 3) the coatings possess distinctly different sets of MFP values. It can bee seen that the MFP of C-2 range from ~20% to 55%, whereas C-5 has MFP values in the range ~45–75%, and Fig. 10 clearly shows that C-5 has a superior adhesion strength to C-2. The additional amount of melt fraction C-5 is believed to enhance adhesion strength through improving the inter-lamellae contact in the coating. On the other hand, the Young's modulus value of C-4 is higher than C-6 and C-7 (Fig. 10). Again, this can be related to MFP values. It can be seen that the measured MFP values for C-4 lies in the range 20–60%. C-5 and C-6, however, contain MFP values in the range 40–80%. It appears that a relatively lower MFP value, which corresponds to a higher HA content, is a significant contributing factor to the stiffness of the coating.

Indeed, Fig. 5 shows that the TCP content for C-5 is higher than the TCP content in C-4. The Young's moduli values were obtained by 3-point bend test, and it had been reported in a previous publication [31]. Finally, it was found that there is no significant difference in the fracture toughness of the coatings C-4, C-5 and C-6 (0.48–0.51 MPa $m^{0.5}$). This may be due to the possibility that fracture behavior in thermal sprayed coatings is contingent on inter-lamellae voids and porosities, rather than phase content. Therefore, the melt fraction does not exert any noticeable influence.

4. Conclusion

The 'melt fraction in particle' (MFP) of HVOF sprayed HA powder was experimentally determined in the present study. Results showed that the powders have MFP values in the range ~20–100%. It was found that the MFP values corresponded to the starting powder size and HVOF spray parameters. The extent of HA thermal decomposition in the HVOF spray was significantly reflected through the melt state of the powders. Furthermore, in vitro evaluation confirmed that the melted portion of HA splats markedly dissolve more readily than the un-melted part. Nanoindentation test on as sprayed HA particles and coatings revealed that different phases resulted from thermal decomposition of HA contributed to the overall Young's modulus value. A key influence of the melt state of HA powders during HVOF spraying to form a coating was revealed through the coatings' tensile adhesive strength and Young's modulus.

Acknowledgements

The authors would like to thank Ms. Kiatkiat Lim, Ms. Jovice Ng, and Mr. Tan Boon Leng for their help in the sample preparation. They also thank Dr. Luca Lutterotti from Universita di Trento of Italy for his permission to use the Rietquan program in quantitatively analyzing the phases in coating samples. The financial support by Nanyang Technological University through JT ARC 4/96 is also acknowledged.

References

[1] Oonishi H, Yamamoto M, Ishimau H, Tsuji E, Kushitani S, Aono M, Ukon Y. The effect of hydroxyapatite coating on bone growth into porous titanium alloy implants. J Bone Jt Surg 1989;10:213–6.
[2] Hardy D, Frayssinet P, Delince P. Osteointegration of hydroxyapatite-coated stems of femoral prostheses. Eur J Orthop Surg Traumatol 1999;9:75–81.
[3] Wang B, Chang E, Yang C. Characterization of plasma-sprayed bioactive hydroxyapatite coatings in vitro and in vivo. Mater Chem Phys 1994;37:55–63.
[4] Tranquilli P, Merolli A, Palmacci Q, Gabbi C, Cacchiloli A, Gonizzi G. Evaluation of different preparations of plasma-spray hydroxyapatite coating on titanium alloy and duplex stainless steel in the rabbit. J Mater Sci Mater Med 1994;5:345–9.
[5] Klein C, Wolke J, de Blieck-Hogervorst J, de Groot K. Calcium phosphate plasma-sprayed coatings and their stability: an in vivo study. J Biomed Mater Res 1994;28:909–17.
[6] Ong J, Chan D. Hydroxyapatite and their use as coatings in dental implants: a review. Crit Rev Biomed Eng 2000;28:667–707.
[7] Fazan F, Marquis P. Dissolution behavior of plasma-sprayed hydroxyapatite coatings. J Mater Sci Mater Med 2000;11:787–92.
[8] Grassmann O, Heimann R. Compositional and microstructural changes of engineered plasma-sprayed hydroxyapatite coatings on Ti6Al4V substrates during incubation in protein-free simulated body fluid. J Biomed Mater Res 2000;53:685–93.
[9] Nagano M, Nakamura T, Kokubo T, Tanahashi M, Ogawa M. Differences of bone bonding ability and degradation behaviour in vivo between amorphous calcium phosphate and highly crystalline hydroxyapatite coating. Biomaterials 1996;17:1771–7.
[10] Paschalis E, Zhao Q, Tucker B, Mukhopadhayay S, Bearcroft J, Beals N, Spector M, Nancollas G. Degradation potential of plasma-sprayed hydroxyapatite-coated titanium implants. J Biomed Mater Res 1995;29:1499–505.
[11] Hing K, Best S, Bonfield W. Characterization of porous hydroxyapatite. J Mater Sci Mater Med 1999;10:135–45.
[12] Yang C, Lin R, Wang B, Lee T, Chang E, Hang Y, Chen P. In vitro and in vivo mechanical evaluations of plasma-sprayed hydroxyapatite coatings on titanium implants: the effect of coating characteristics. J Biomed Mater Res 1997;37:335–45.
[13] Cleries L, Fernandez-Pradas J, Morenza J. Behavior in simulated body fluid of calcium phosphate coatings obtained by laser ablation. Biomaterials 2000;21:1861–5.
[14] Gross K, Berndt C. Thermal processing of hydroxyapatite for coating production. J Biomed Mater Res 1998;39:580–7.
[15] Ogiso M, Yamashita Y, Matsumoto T. Differences in microstructural characteristics of dense HA and HA coating. J Biomed Mater Res 1998;41:296–303.
[16] Gross K, Berndt C, Herman H. Amorphous phase formation in plasma-sprayed hydroxyapatite coatings. J Biomed Mater Res 1998;39:407–14.
[17] Tadnno S, Shibano M, Ukai J. Residual stress evaluation of hydroxyapatite coating Ti implant. J Solid Mech Strength Mater 1997;40:328–35.
[18] Brown S, Turner I, Reiter H. Residual stress measurement in thermal sprayed hydroxyapatite coatings. J Mater Sci Mater Med 1994;5:756–9.
[19] Brown S, Turner I. Acoustic emission analysis of thermal sprayed hydroxyapatite coatings examined under four-point bend loading. Surf Eng 1998;14:309–13.
[20] Bianchi L, Leger A, Vardelle M, Vardelle A, Fauchais P. Splat formation and cooling of plasma-sprayed zirconia. Thin Solid Films 1997;305:35–47.
[21] Montavon G, Sampath S, Berndt C, Herman H, Coddet C. Effects of vacuum plasma spray processing parameters on splat morphology. J Therm Spray Technol 1995;4:67–74.
[22] Gougeon P, Moreau C. Simultaneous independent measurement of splat diameter and cooling time during impact on a substrate of plasma-sprayed molybdenum particles. J Therm Spray Technol 2001;10:76–82.
[23] Kweh S, Khor K, Cheang P. Production and characterization of hydroxyapatite (HA) powders. J Mater Process Technol 1999; 89–90:373–7.
[24] Young R. The Rietveld method, International Union of Crystallography. New York: Oxford University Press; 1993.
[25] Rietveld H. Line profiles of neutron powder-diffraction peaks for structure refinement. Acta Cryst 1967;22:151–2.

[26] H. Li, HVOF spraying of hydroxyapatite and hydroxyapatite/titania composites. PhD thesis. Nanyang Technological University, 2002.
[27] Kokubo T, Kushitani H, Sakka S, Kitsugi T, Yamamuro T. Solutions able to reproduce in vivo surface changes in bioactive glass–ceramic A–W[3]. J Biomed Mater Res 1990;24:721–4.
[28] Oliver W, Pharr G. An improved technique for determining hardness and elastic modulus using load and displacement sensing indentation experiments. J Mater Res 1992;7:1564–83.
[29] Woirgard J, Cabioch T, Riviere J, Dargenton J. Nanoindentation characterization of SiC coatings prepared by dynamic ion mixing. Surf Coat Technol 1998;100–101:128–31.
[30] Chicot D, Hage I, Demarecaux P, Lesage J. Elastic properties determination from indentation tests. Surf Coat Technol 1996;81:269–74.
[31] Li H, Khor K, Cheang P. Young's modulus and fracture toughness determination of HVOF sprayed bioceramic coatings. Surf Coat Technol 2002;155:21–32.
[32] D. Poulikakos, Conduction heat transfer. Englewood Cliffs, NJ: Prentice-Hall International Editions, 1994.
[33] Wang Y, Khor K, Cheang P. Thermal spraying of functionally graded calcium phosphate coatings for biomedical implants. J Therm Spray Technol 1998;7:50–7.
[34] McPherson R, Gane N, Bastow T. Structural characterization of plasma-sprayed hydroxylapatite coatings. J Mater Sci Mater Med 1995;6:327–34.
[35] Radin S, Ducheyne P. The effect of plasma sprayed induced changes in the characteristics on the in vitro stability of calcium phosphate ceramics. J Mater Sci 1992;3:33–42.
[36] Cao Y, Weng J, Chen J, Feng J, Yang Z, Zhang X. Water vapour-treated hydroxyapatite coatings after plasma spraying and their characteristics. Biomaterials 1996;17:419–24.
[37] Girardin E, Millet P, Lodini A. X-ray and neutron diffraction studies of crystallinity in hydroxyapatite coatings. J Biomed Mater Res 2000;49:211–5.
[38] Liao C, Lin F, Chen K, Sun J. Thermal decomposition and reconstitution of hydroxyapatite in air atmosphere. Biomaterials 1999;20:1807–13.
[39] Zhou J, Zhang X, Chen J, Zeng S, de Groot K. High temperature characteristics of synthetic hydroxyapatite. J Mater Sci Mater Med 1993;4:83–5.
[40] American Ceramic Society. Phase diagrams for ceramists, vol. 5. Washington, DC: American Ceramic Society, 1983.
[41] Wang B, Chang E, Yang C, Tu D, Tsai H. Characteristics and ostoconductivity of three different plasma-sprayed hydroxyapatite coatings. Surf Coat Technol 1993;58:107–17.
[42] Mihailova B, Kolev B, Balarew C, Dyulgerova E, Konstantinov L. Vibration spectroscopy study of hydrolyzed precursors for sintering calcium phosphate bio-ceramics. J Mater Sci 2001;36:4291–7.
[43] Penel G, Leroy G, Rey C, Sombret B, Huvenne J, Bres E. Infrared and Raman microspectrometry study of fluor-fluor-hydroxy and hydroxy-apatite powders. J Mater Sci Mater Med 1997;8:271–6.
[44] Aoki H. Medical applications of hydroxyapatite. Tokyo, St Louis: Ishiyaku EuroAmerica, Inc.; 1994.
[45] Ducheyne P, Radin S, King L. The effect of calcium phosphate ceramic composition and structure on in vitro behaviour: I. dissolution. J Biomed Mater Res 1993;17:25–34.
[46] Gross KA, Ben-Nissan B, Walsh WR, Swarts E. Analysis of retrieved hydroxyapatite coated orthopaedic implants. In: Coddet C, editor. Thermal Spray: Meeting the Challenges of the 21st Century, Proceedings of the 15th International Thermal Spray Conference, Nice, France, May 1998. p. 1133–8.